2011 IEEE/RSJ International Conference on
Intelligent Robots and Systems
September 25-30, 2011. San Francisco, CA, USA

Instantaneous Stiffness Effects on Impact Forces in Human-Friendly Robots

Dongjun Shin[1], Zhan Fan Quek[2], Samson Phan[2], Mark Cutkosky[2], and Oussama Khatib[1]

[1]*Artificial Intelligence Laboratory, Stanford University, Stanford, CA 94305, USA*
{djshin, ok}@robotics.stanford.edu
[2]*Biomimetic and Dexterous Manipulation Laboratory, Stanford University, Stanford, CA 94305, USA*
{zfquek, sphan, cutkosky}@stanford.edu

***Abstract*— Joint stiffness plays an important role in both safety and control performance, particularly in human-friendly robots using artificial pneumatic muscles. Due to the limited control bandwidth of pneumatic muscles, stiffness characteristics and their effects on safety in the frequency domain should be taken into account. This paper introduces the concept of instantaneous stiffness and validates its model with the Stanford Safety Robot ($S2\rho$). The potential effects of instantaneous stiffness on safety is explored through experimental comparison of peak impact accelerations under various impact conditions. Instantaneous stiffness demonstrates different effects on the impact acceleration depending on impact velocity and controller gain. Finally, the paper discusses the stiffness characteristics as a guideline for design and control to improve the robot safety while maintaining the control performance.**

I. Introduction

Robots are becoming increasingly common and new robotic platforms are being created in environments where interactions with humans will be commonplace. Therefore, robot manipulators must be safe in human proximity. Although ISO 10218-1 was developed to regulate these new robots in order to reduce the likelihood of injury, this strict regulation restricts robot performance to the extent that it is not feasible to achieve fairly fast motion [8]. To prevent injury during operation beyond mandated limits, many researchers have proposed inherently safe robots whose open-loop characteristics are such that no harm could befall humans interacting with them.

A. Safety Criteria

There is considerable research regarding the development of appropriate injury criteria for human-robot collisions. Developed for the automotive industry, the Head Injury Criteria (HIC) is among the most widely used methods for quantifying such collisions. It is based on a time-averaged translational acceleration of the center of mass. A number of researchers have explored inertia, velocity, and their relation to HIC values [6], [17]. Another often used collision quantification metric is peak impact forces. Higher peak forces would most likely result in higher likelihood of injury. Zinn derived the Manipulator Safety Index (MSI) using peak impact acceleration and compared the safety among the manipulators as shown in the following equation [16]:

$$MSI = \Delta t \left[\frac{2}{g\Delta t} \left(\frac{I_a}{I_a + I_h} \dot{x}_{a0} sin(w_n \frac{\Delta t}{2}) \right) \right]^{2.5} \quad (1)$$

$$w_n = \sqrt{\frac{I_a + I_h}{I_a I_h} K_e}$$

where $\dot{x}_{a0}$, I_a, I_h, and K_e are impact velocity, manipulator effective inertia, head effective inertia, and effective interface stiffness, respectively. As shown in Eq. 1, the danger of a robotic platform is believed to be proportional to velocity, manipulator effective inertia, and stiffness. Velocity regulation seems the simplest way to ensure robot safety without changing robot design and control. However, since the velocity regulation (i.e., ISO 12018) in turn results in restricted performance, recent research of robot safety has mainly focused on inertia reduction and stiffness variation.

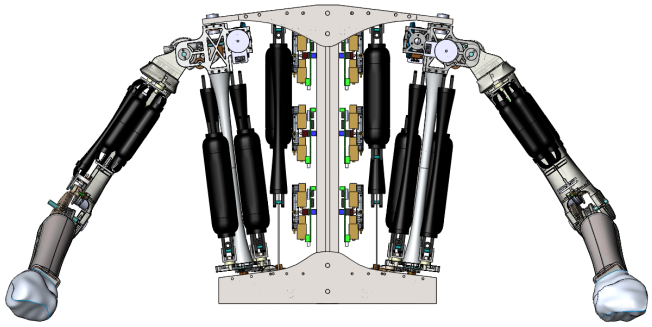

Fig. 1. New Stanford Safety Robot ($S2\rho$)

B. Stanford Safety Robot: Low Inertia for Robot Safety

Inertia reduction is a common method for reducing impact forces. Lighter robot manipulators are less likely to cause injury for a given speed. From the equation of effective inertia

$$I_{eff} = I_{link} + (GearRatio)^2 I_{motor} \quad (2)$$

This has led to the use of direct drive electromagnetic motors for less actuator inertia [1] or relocation of motors to the base using cables for less link inertia [9]. DLR's LWR III employed light structure [7] with Joint Torque Control

(JTC), which allows for near zero output impedance at low frequencies [14].

Pneumatic Artificial Muscles (PAMs) provide high force-to-weight ratio, but their low bandwidth and nonlinear behavior have prevented them from seeing widespread use in traditional robotic designs. However, PAMs' inherent compliance along with an advanced control suggests its potential use in human-safe robot in order to decouple link inertias and consequently reduce impact forces. As is shown in the Stanford Safety Robot ($S2\rho$) developed at Stanford AI Lab, hybrid actuation combining PAMs and high bandwidth electromagnetic motor in parallel compensates for low performance without compromising robot safety [10], [11].

Typical robot manipulators are constructed of relatively stiff and heavy metals, such as aluminum or steel. Such material selection results in more powerful motor, higher effective inertia, and higher contact modulus. Shape Deposition Manufacturing (SDM) allows the $S2\rho$ to be constructed of lightweight polymers in order to reduce effective inertia. Polymer use also reduces the effective contact modulus, further reducing impact forces [15].

C. Stiffness Effect on Robot Safety

Reducing interface stiffness is another method to significantly reduce impact forces [6], [15]. Such interface stiffness can be achieved through selection of less rigid structural material at a cost of pointing accuracy or through compliant coverings which may only affect the bulk.

On the other hand, joint stiffness plays an important role in both robot safety and control performance. It is believed that high stiffness provides better position control performance, yet increases impact force. This trade-off leads to variable stiffness actuation in many robotic manipulators in order to achieve safety without compromising the performance of the system [2], [3]. However, Haddaddin et al. noted that the joint stiffness has little effect on HIC collision values [6]. Van Damme et al. also confirmed that joint stiffness has very limited effect on impact force [13].

Since control bandwidth limitation results in frequency-variant joint stiffness, the analysis of the frequency-variant stiffnesses in various conditions is essential to further understand the stiffness effects on robot safety. Furthermore, comprehension of these stiffness characteristics allows for enhanced controller and mechanism designs that improve control performance. Section II presents an effective stiffness model describing the stiffness variation over frequency. Section III describes an experimental setup in $S2\rho$ testbed. Section IV provides the identification and validation of the instantaneous stiffness and analyzes stiffness effects on impact acceleration. Finally, Section V discusses the model limitation due to friction and design suggestion based on the result analysis.

II. Instantaneous Stiffness as a Function of Frequency

A time-domain impact model does not reflect stiffness variation with respect to frequency and thus cannot provide proper evaluation of safety, especially at high impact velocity. To eliminate this shortcomings, we developed an instantaneous stiffness model combining an inherent stiffness generated by PAMs and active stiffness produced by a controller in the frequency domain. The instantaneous stiffness model can be integrated into an impact model in order to validate manipulator safety. The proposed stiffness model enables an impact model to describe correct behavior under variation of stiffness with respect to impact velocity and controller gain. Key variables in this paper are listed in Table I.

Unlike the simple passive (spring) stiffness, controller-based stiffness and the inherent stiffness by PAMs are

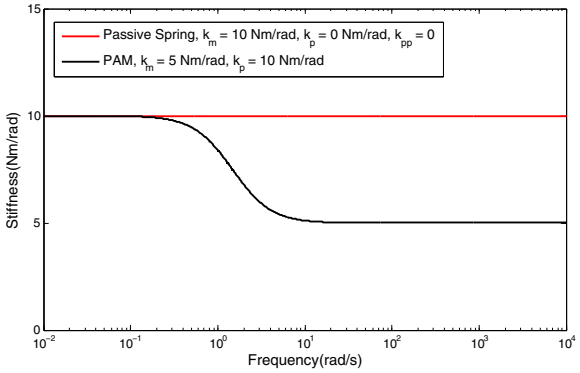

(a) Joint stiffness w.r.t stiffness sources

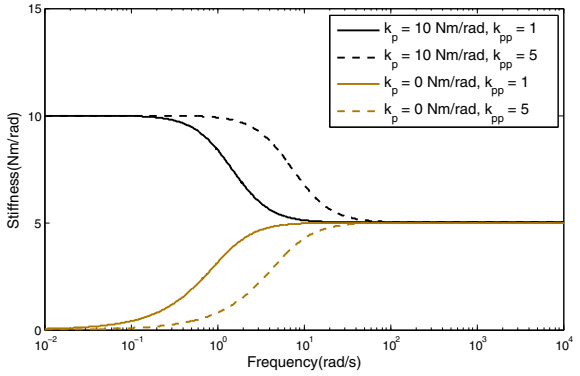

(b) Stiffness of a PAMs-driven joint w.r.t k_p and k_{pp}

Fig. 2. (a) While the stiffness of a pneumatic muscle-driven joint rolls off at its position control bandwidth, purely passive spring joint (no controller) mimics a lumped parameter model with a frequency-invariant stiffness value. (b) In case of a PAM-driven joint, the effective stiffness matches k_p at a low frequency, but k_m determines the effective stiffness at a high frequency. Meanwhile, k_{pp} determines the frequency at which this transition occurs.

Variable	Definition	Units
k_{eq}	Effective joint stiffness	Nm/rad
k_m	Joint stiffness by PAMs	Nm/rad
k_{int}	Interface stiffness	N/m
k_{pp}	Force control gain	
k_p	Position control gain	Nm/rad
$\dot{x}_l$	Impact velocity	m/sec

TABLE I
Key Variables

variable with respect to frequency due to their bandwidth limitations. The active stiffness in an electromagnetically powered joint can be zero at high frequencies [6], because a stiffness starts to roll off near a position control bandwidth. On the other hand, the stiffness of a joint torque control is ideally zero, as no position control gain is involved. However, the deviations and disturbances of the muscle forces due to bandwidth limitation can instantaneously generate joint stiffness. This instantaneous joint stiffness typically occurs at higher frequencies than the force control bandwidth.

In order to derive the effective stiffness capturing the instantaneous stiffness, the impedance of a pneumatic-muscles-driven joint is derived as follows:

$$\begin{aligned} \frac{\tau_{ext}(s)}{\theta(s)} &= I_{eff}s^2 + Bs + k_m + \frac{k_{pp}E}{s + k_{pp}E}(k_p - k_m) \quad (3) \\ k_m &= \frac{P_0 b^2}{4\pi n^2}\left(\frac{6L_0}{b^2}\right)2R^2 \\ E &= \frac{b^2}{4\pi n^2}\left(\frac{3L_0^2}{b^2} - 1\right) \end{aligned}$$

where k_p and k_{pp} are position controller gain and force controller gain, respectively. P_0, L_0, and R are initial muscle pressure, initial muscle length, and pulley radius, respectively. b and n are muscle constants [4]. See Appendix for the detailed equations. The joint effective stiffness representing instantaneous stiffness is

$$k_{eq} = k_m + \frac{k_{pp}E}{s + k_{pp}E}(k_p - k_m) \quad (4)$$

The roll-off frequency of the effective stiffness is determined by the muscle properties, E, and force controller gain, k_{pp}, of the pneumatic muscle. Fig. 2 (a) shows the frequency-variant joint stiffness with respect to different stiffness sources. While the stiffness of a pneumatic muscle-driven joint depends on its position control bandwidth, purely passive spring joint provides a frequency-invariant stiffness since its stiffness is not affected by any controller. Fig. 2 (b) shows the effective stiffness of PAM-driven joint with various controllers. The effective stiffness matches k_p at a low frequency, but k_m sets the effective stiffness at a high frequency. Meanwhile, k_{pp} determines the frequency at which this transition occurs. In a slow arm movement, which is the event below the position control bandwidth, the second term in Eq. 4 approaches $(k_p - k_m)$, and thus the effective stiffness becomes k_p. Of course, no position controller, i.e., $k_p = 0$, results in marginal stiffness in the slow movement. However, when the arm is moved instantaneously, higher stiffness may be induced (if k_p is higher than k_m). Eq. 4 explains this behavior in that effective stiffness increases and converges to k_m as the second term in Eq. 4 becomes lower as the frequency increases.

III. Experimental Setup

In order to explore the stiffness effect on safety in terms of impact acceleration, we employ the $S2\rho$ testbed (Fig. 3 [11]), where we also validate and identify the instantaneous stiffness. We moved the arm from rest with various k_m and k_{pp} for the identification of the instantaneous stiffness, using the attached mini motor in the $S2\rho$ testbed to provide the step external torque input. The instantaneous stiffness is identified by the following equation

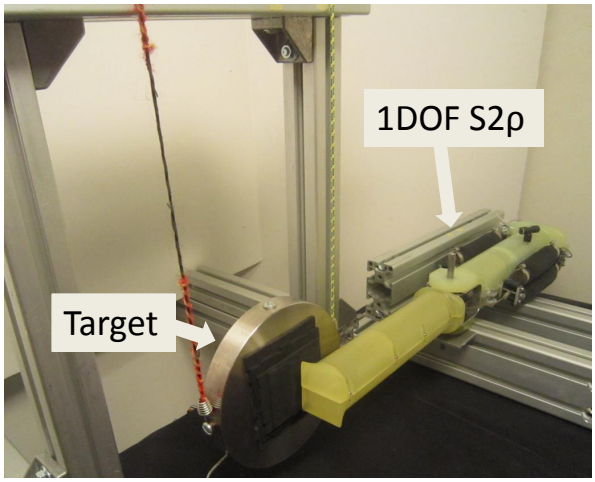

Fig. 3. Experimental setup [11]. The target consists of a steel mass covered in compressible foam (k_{int} = 37 kN/m) whose mass matches that of a 50^{th} percentile male head and neck (6 kg) [5]. Active stiffness, semi-passive stiffness have been achieved by position controller, antagonistic pair of pneumatic muscles, respectively.

$$\begin{aligned} k_{eq} &= \frac{\tau_{ext}}{\theta} \quad (5) \\ &= k_m + \frac{k_{pp}E}{s + k_{pp}E}(k_p - k_m) \end{aligned}$$

where τ_{ext} is the external joint torque measured by the load cell, and θ is the angle away from the equilibrium position, measured by the encoder. In another experiment, the $S2\rho$ arm is used to impact against a steel mass target covered in compressible foam (k_{int} = 37 kN/m) whose mass matches that of a 50^{th} percentile male head and neck (6 kg) [5]. The head mass is outfitted with an accelerometer, whose measurements are plotted in the results section. For each test, the manipulator is velocity controlled through the target location. For both experiments, the robotic arm is rigidly mounted in such a way that the path of movement is perpendicular to gravity, thus reducing the effect it may have on collision dynamics.

IV. Results

A. Identification of Instantaneous Stiffness

The instantaneous stiffness diminishes as the impact frequency increases. Fig. 4 (a) shows that the instantaneous joint stiffness is induced in proportion to k_m, then decreases to zero as a force controller compensates for force error. Note that under this experiment, since the system is under force control and its position is not controlled, the position control gain k_p is equal to 0. In addition, the nonzero steady-state stiffness in case of high k_m is caused not by actual stiffness

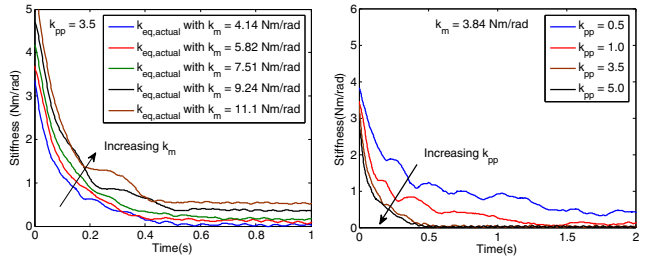

(a) Stiffness w.r.t. k_m over time (b) Stiffness w.r.t. k_{pp} over time

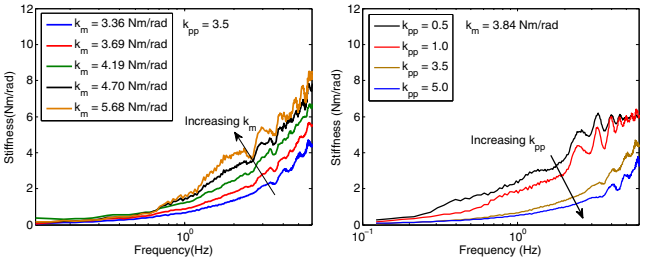

(c) Stiffness w.r.t. k_m over freq. (d) Stiffness w.r.t. k_{pp} over freq.

Fig. 4. (a) When a joint starts to move, instantaneous joint stiffness appears rapidly due to the limitation of the force control of PAMs. (b) Since the stiffness diminishes as the force controller eliminates the force error, a higher control gain reduces the instantaneous stiffness faster. (c) Effective stiffness approaches to k_m as the frequency increases. (d) At a low frequency, a higher controller gain further decreases the stiffness, while, at a high frequency, the stiffness eventually converges to k_m no matter what controller gain is used.

but by hysteresis due to high pressure. Since the limitation of the force control of PAMs results in instantaneous stiffness, higher performance controller decreases the stiffness faster as the controller better eliminates the force error, as is shown in Fig. 4 (b).

Fig. 4 (c) and (d) show the effective stiffness in the frequency domain. While, at a low frequency, the stiffness converges to zero thanks to the joint torque control, the stiffness approaches to k_m at a high frequency due to the control bandwidth limitation. Fig. 4 (d) represents that a higher controller gain further decreases the stiffness at a low frequency, while, at a high frequency, the stiffness eventually converges to k_m no matter what controller gain is used.

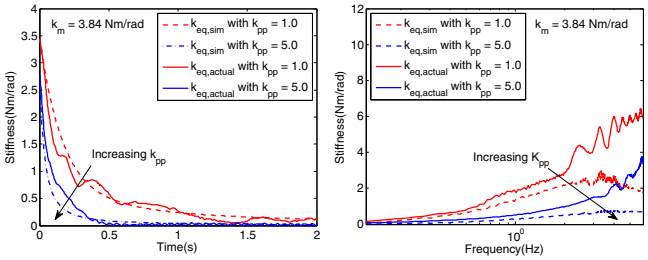

(a)Model validation in the time domain (b) Model validation in the frequency domain

Fig. 5. (a) The model matches experimental results at the moment of movement. However, due to the friction, actual stiffness converges zero slower than that of model. (b) High k_{pp} reduces the deviation from the model, since this allows for lower force error.

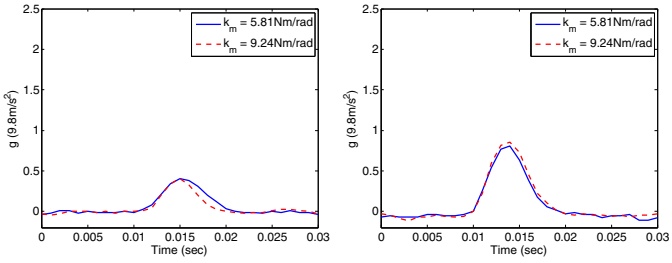

(a) Impact velocity 0.4 m/s (b) Impact velocity 0.8 m/s

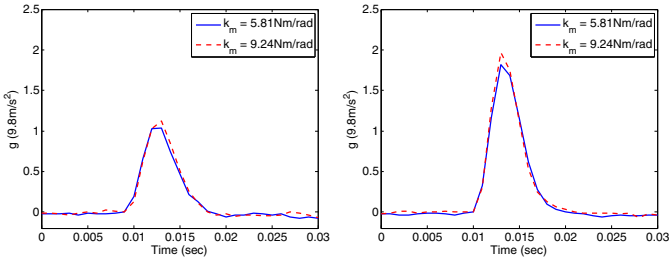

(c) Impact velocity 1.2 m/s (d) Impact velocity 1.6 m/s

Fig. 6. Impact acceleration with respect to k_m given impact velocity. Higher stiffness does not significantly increase the impact acceleration, while showing almost the same influence on impact acceleration as lower stiffness does at a low impact velocity.

In addition, Fig. 5 shows that the effective stiffness model derived in Section II captures the real behavior of instantaneous stiffness. However, since we have measured the stiffness through joint displacements, the measurement is under influence of open-loop position control bandwidth. Hence, the measured stiffness is expected to be higher than theoretical stiffness due to friction in particular at a high frequency and/or at a high muscle stiffness. Higher k_{pp}

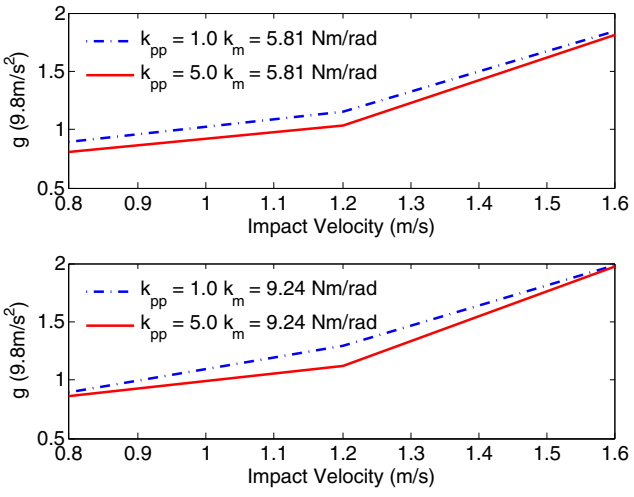

Fig. 7. Impact acceleration with respect to k_m and k_{pp}, given impact velocity. Since higher k_{pp}, further and more quickly decreases the instantaneous stiffness, the impact acceleration is lower than that of lower k_{pp}. However, at a high impact velocity, peak accelerations are almost identical since the instantaneous stiffness converges to the same k_m no matter what k_{pp} is used.

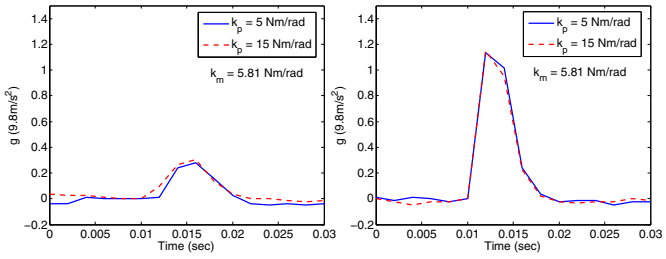

(a) $\dot{x}_l$ = 0.4 m/s (b) $\dot{x}_l$ = 1.2 m/s

Fig. 8. Impact acceleration with respect to active stiffness by position close-loop controller, k_p. Higher k_p marginally ($\sim$ 9 %) increases the impact acceleration only at a fairly low impact velocity due to the limited position control bandwidth.

reduces this deviation from the model, since this allows for lower force error.

B. Instantaneous Stiffness Effects on Safety

We have measured impact acceleration as an indicator of robot safety with respect to the joint stiffness produced by different sources such as an position controller and pneumatic muscles.

At the impact velocities of equal to or higher than 0.8 m/s, higher k_m increases the impact acceleration, but the differences are not significant, as is shown in Fig. 6. Furthermore, the stiffness does not seem critical to the impact force in particular at a low impact velocity since instantaneous stiffness quickly drops as explained in Section II.

Fig. 7 illustrates how the force controller of the PAM, k_{pp}, affects the robot safety. Since higher k_{pp} further/quicker decreases the instantaneous stiffness, the impact acceleration is lower than it is for lower k_{pp}. However, at a high impact velocity, the peak accelerations are almost identical since control bandwidth limitation have instantaneous stiffness converged to the same k_m no matter what controller gain is used.

Fig. 8 shows impact acceleration with respect to active stiffness generated by position close-loop controller, k_p. Higher k_p marginally increase the impact acceleration beyond the impact velocity of 1.2 m/s, due to the limited position control bandwidth.

V. Conclusion and Discussion

We derived an effective stiffness model describing an instantaneous (high frequency) stiffness. Then we validated the effective stiffness model in an antagonistic-muscle driven joint and analyzed the identified stiffness in both the time and frequency domains. At the moment of initial joint movement, an effective stiffness instantaneously increases proportional to the joint stiffness generated by PAMs due to the limitation of force control bandwidth. As the controller reduces the force error, the effective stiffness eventually becomes near zero at the convergence rate, which a force controller gain determines. Note that the amplitude of the instantaneous stiffness depends on the joint stiffness produced by PAMs. Analysis in the frequency domain validates that higher controller gain further reduces the effective stiffness within the force control bandwidth. Beyond that bandwidth, the effective stiffness converges regardless of the controller gain.

In addition, we investigated the stiffness effects on impact force in a human-friendly robot testbed. Generally, the stiffness effects on the impact force is not significant such that higher joint stiffness generated by PAMs increases impact force less than 10 percent. Rather, a fairly fast force control effectively reduces the instantaneous stiffness, and thus impact force. However, the control bandwidth limitation offsets this advantage at high velocity impact. In addition, the reduced active stiffness by the position controller meaningfully decreases impact force only at frequencies lower than its position control bandwidth, which is typically lower than force control bandwidth.

Instantaneous Stiffness Effects on Performance

From the results, we are able to decouple robot performance from robot safety when it comes to determining the inherent stiffness by PAMs and position control gain. In other words, we can choose these parameters solely for robot performance since these affect robot safety only at a low impact velocity, where safety is mostly not a critical issue. While an appropriate force controller improves both robot safety and performance, the effect on safety is limited in particular at a high impact velocity, where the manipulator effective inertia and interface stiffness have dominant effects on impact force.

In this regard, a strategy to deal with the frequency-variant instantaneous stiffness needs to be investigated for better control performance. The stiffness introduces nonlinear factors over a wide frequency range, and may cause interference between actuators, particularly in the hybrid actuation [12]. We will provide a solution to negate the instantaneous stiffness by a novel transmission and control algorithm.

Further investigation of a friction model and a valve model will probably help the model accuracy, and thus reduce the deviation of the experimental data from the stiffness model at high muscle stiffness. This is because high muscle stiffness is generated by high pressure of muscle, which increases muscle internal friction nonlinearly. Additionally, since interface stiffness substantially varies during impact, a future model will include the relationship between impact velocity and interface stiffness. High impact velocity can quickly squeezes interface material, and thus increases its stiffness instantaneously.

VI. Acknowledgments

We are gratefully acknowledge the generous advice and comments of members of the Stanford Artificial Intelligence Laboratory and the Biomimetic Dexterous Manipulation Laboratory.

APPENDIX

Effective Stiffness Model

The equation of motion of a 1-DOF robotic arm with antagonistic pneumatic muscle pairs is given by

$$I_{eff}\ddot{\theta} + B\dot{\theta} = R(f_1 - f_2) + \tau_{ext} \tag{6}$$

in which the forces by agonistic and antagonistic muscles are given by the relations

$$f_1 = \frac{P_1 b^2}{4\pi n^2}\left(\frac{3(L_0 - R\theta)^2}{b^2} - 1\right) \tag{7}$$

$$f_2 = \frac{P_2 b^2}{4\pi n^2}\left(\frac{3(L_0 + R\theta)^2}{b^2} - 1\right) \tag{8}$$

We assume the pressure dynamics with force control are given by the equations

$$\dot{P_1} = k_{pp}k_{valve}(f_{1,d} - f_1); \tag{9}$$

$$\dot{P_2} = k_{pp}k_{valve}(f_{2,d} - f_2); \tag{10}$$

where k_{valve} is an empirically obtained variable of valve characteristics. The desired forces under the hybrid macro-mini actuation scheme are given by

$$f_{1,d} = f_0 + \frac{k_p}{2R}(\theta_d - \theta) \tag{11}$$

$$f_{2,d} = f_0 - \frac{k_p}{2R}(\theta_d - \theta) \tag{12}$$

Linearizing the above formulation about $\theta = \theta_0$ with $P_1 = P_{1,0}, P_2 = P_{2,0}$, and taking the Laplace transform, we obtained

$$\frac{\theta(s)}{\tau_{ext}(s)} = \frac{1}{I_{eff}s^2 + Bs + k_{eq}} \tag{13}$$

in which

$$k_{eq} = C\frac{s}{s + k_{pp}E} + D\frac{s}{s + k_{pp}F} + \frac{1}{2}\frac{k_{pp}E}{s + k_{pp}E} + \frac{1}{2}\frac{k_{pp}F}{s + k_{pp}F}$$

and the coefficients C, D, E and F are

$$C = \frac{R^2 P_{1,0} b^2}{4\pi n^2}\frac{6(L_0 - R\theta_0)}{b^2}$$

$$D = \frac{R^2 P_{2,0} b^2}{4\pi n^2}\frac{6(L_0 + R\theta_0)}{b^2}$$

$$E = \frac{b^2 k_{valve}}{4\pi n^2}\left(\frac{3(L_0 - R\theta_0)^2}{b^2} - 1\right)$$

$$F = \frac{b^2 k_{valve}}{4\pi n^2}\left(\frac{3(L_0 + R\theta_0)^2}{b^2} - 1\right)$$

C and D are the passive stiffness provided by the upper and lower muscle respectively. For the case when $P_{1,0} = P_{2,0} = P_0$ and $\theta_0 = 0$,

$$C = D = \frac{1}{2}k_m, \qquad E = F$$

Therefore,

$$k_{eq} = k_m\frac{s}{s + k_{pp}E} + k_p\frac{k_{pp}E}{s + k_{pp}E}$$

$$= k_m + \frac{k_{pp}E}{s + k_{pp}E}(k_p - k_m)$$

REFERENCES

[1] H. Asada and T. Kanade. Design of direct drive mechanical arms. *ASME Journal of Vibration, Acoustics, Stress, and Reliability in Design*, 105:312–316, July 1983.

[2] A. Bicchi and G. Tonietti. Fast and soft-arm tactics. *IEEE Robotics and Automation Magazine*, 11(2):22–33, 2004.

[3] J. Choi, S. Park, W. Lee, and S. Kang. Design of a robot joint with variable stiffness. *2008 IEEE International Conference on Robotics and Automation*, pages 1760–1765, May 2008.

[4] C. P. Chou and B. Hannaford. Measurement and modeling of mckibben pneumatic artificial muscles. *IEEE Robotics and Automation Magazine*, 12(1):90–102, 1996.

[5] V. Gowdy, R. DeWeese, M. Beebe, B. Wade, J. Duncan, R. Kelly, and J.L. Blaker. A lumbar spine modification to the hybrid iii atd for aircraft seat tests. *SAE Technical paper series*, 1999.

[6] S. Haddadin, A. Albu-Schaffer, and G. Hirzinger. Safe Physical Human-Robot Interaction:Measurements, Analysis and New Insights. Hiroshima, Japan.

[7] G. Hirzinger, N. Sporer, A. Albu-Schaffer, M. Hahnle, and A. Pascucci. Dlr's torque-controlled light weight robot iii - are we reaching the technological limits now? *In Proc. of the Intl. Conf. on Robotics and Automation, Washington, DC*, pages 1710–1716, 2002.

[8] ISO10218. Robots for industrial environments - safety requirements - part 1: Robot. 2011.

[9] K. Salisbury, W. Townsend, B. Ebrman, and D. DiPietro. *Preliminary design of a whole-arm manipulation system (WAMS)*. IEEE Comput. Soc. Press.

[10] D. Shin, I. Sardellitti, and O. Khatib. A hybrid actuation approach for human-friendly robot design. *Proc. of the 2008 IEEE International Conference on Robotics and Automation*, pages 1747–1752, 2008.

[11] D. Shin, I. Sardellitti, Y. Park, O. Khatib, and M. Cutkosky. Design and control of a bio-inspired human-friendly robot. *The International Journal of Robotics Research*, 29(5):571–584, 2010.

[12] D. Shin, F. Seitz, O. Khatib, and M. Cutkosky. Analysis of torque capacities in hybrid actuation for human-friendly robot design. *Proc. of the 2010 IEEE International Conference on Robotics and Automation*, pages 799–804, 2010.

[13] M Van Damme, P Beyl, B Vanderborght, R Van Ham, I Vanderniepen, A Matthys, P Cherelle, and D. Lefeber. The role of compliance in robot safety. *Dependable Robots in Human Environments*, 2010.

[14] D. Vischer and O. Khatib. Design and development of high-performance torque-controlled joints. *IEEE Trans. on Robotics and Automation*, 11(4):537–544, 1995.

[15] M. Wassink and S. Stramigioli. Towards a novel safety norm for domestic robotics. In *Intelligent Robots and Systems, 2007. IROS 2007. IEEE/RSJ International Conference on*, pages 3354–3359, 2007.

[16] M. Zinn. *A New Actuation Approach for Human-Friendly Robotic Manipulation*. Thesis (phd).

[17] M. Zinn, B. Roth, O. Khatib, and J. K. Salisbury. New actuation approach for human-friendly robot design. *International Journal of Robotics Research*, 23(1):379–398, 2004.